Muon-neutrino carbon charged-current interaction near the muon threshold

D. D. Koetke, R. Fisk, D. S. Koetke,[a] and R. Manweiler
Valparaiso University, Valparaiso, Indiana 46383

T. J. Bowles, A. Brown,[b] R. E. Brown, R. L. Burman, D. A. Clark, S. Clearwater,[c]
T. Dombeck,[b] H. Kruse, and D. Lee
Los Alamos National Laboratory, Los Alamos, New Mexico 87545

B. Aas[d] and G. Igo
University of California, Los Angeles, California 90024

C. Newsom
University of California, Los Angeles, California
and University of Iowa, Iowa City, Iowa 52242

D. Beavis,[e] S. Y. Fung, W. Gorn, R. T. Poe,[f] and G. J. VanDalen
University of California, Riverside, California 92521

B. Bassalleck, B. Dieterle, C. Gregory, R. E. Hill,[g] J. H. Kang,[h] and C. Leavitt
University of New Mexico, Albuquerque, New Mexico 87131

L. Auerbach, S. Datta,[i] and Y. Huang[j]
Temple University, Philadelphia, Pennsylvania 19122
(Received 5 May 1992)

A measurement of the muon-neutrino carbon charged-current cross section, $^{12}C(\nu_\mu,\mu^-)X$, was performed using the in-flight pion-decay neutrino source at the LAMPF accelerator. At an average interacting neutrino energy of 202 MeV an inclusive cross section of $(15.9\pm2.6\pm3.7)\times10^{-39}$ cm^2 was measured. This value is in best agreement with the Fermi-gas model and is in disagreement with a previous experiment and subsequent calculations that yielded substantially lower cross sections. However, the muon energy spectrum shows a marked depletion of events at high energies compared to the Fermi-gas model. From a small sample of events in which the final-state nucleus was in the ground state of ^{12}N, a cross section for the reaction $^{12}C(\nu_\mu,\mu^-)^{12}N$(g.s.) of $(1.7\pm0.8\pm0.3)\times10^{-39}$ cm^2 or about $11\pm5\%$ of the total event rate was obtained.

PACS number(s): 24.80.−x, 13.10.+q, 14.60.Gh

I. INTRODUCTION

Over the last fifteen years a number of theoretical papers have discussed the neutrino-nuclear interaction at low energies where information can be obtained about the weak vector and axial-vector currents in the nucleus [1,2]. These authors have pointed out that the neutrino study is complementary to experiments using electrons as probes where only the vector part of the interaction is present. Furthermore, low-energy neutrinos interact only with the neutrons in the nucleus, while electrons see only the protons. When exclusive nuclear transitions are involved, one can use the nuclear quantum numbers to learn about the structure of the weak interaction as well as to study weak currents within the nucleus.

The experiment reported in this paper studies the charged-current interaction of muon neutrinos with carbon just above the muon threshold where nuclear effects dominate. Specifically, we report the measurement of the cross sections for the inclusive reaction $^{12}C(\nu_\mu,\mu^-)X$ and for the exclusive process $^{12}C(\nu_\mu,\mu^-)^{12}N$(g.s.). The latter is the first observation of a ν_μ-induced transition between specific nuclear states.

In the case of the inclusive final state, a number of theoretical papers [3,4] have dealt specifically with the neutrino-carbon interaction and have predicted cross sections that vary by large factors. Furthermore, low-energy

[a]Now at Stanford University, Stanford, CA 94305.
[b]Now at SSCL, Dallas, TX 75237.
[c]Now at Xerox Corp., Palo Alto Research Center, Palo Alto, CA 94304.
[d]Now at Rogalandsforskining, N-4001 Stavanger, Norway.
[e]Now at Brookhaven National Laboratory, Upton, NY 11973.
[f]Deceased.
[g]Now at Los Alamos National Laboratory, Los Alamos, NM 87545.
[h]Now at University of California, Riverside, CA 92521.
[i]Now at Fermilab, Batavia, IL 60510.
[j]Now at Albert Einstein College of Medicine, Bronx, NY 10461.

neutrino interactions on nuclei frequently play an important role in experimental searches for neutrino oscillations. A knowledge of these cross sections has likewise become important for underground laboratory experiments attempting to study extraterrestrial sources of neutrinos [5].

Only one other experiment has been performed with a low-energy muon-neutrino beam [6]. In that experiment the Brookhaven Alternating Gradient Synchrotron energy was lowered to 800 MeV, which resulted in low beam currents. They observed only 3 ± 2 neutrino-carbon muon events, while a Fermi gas model (FGM) calculation [3] of the cross section predicted five events. Because a discrepancy with the FGM could be evidence for muon neutrinos oscillating to tau neutrinos, Kim and Mintz [7] re-investigated the older predictions of the cross section. They found that the cross section could be as low as one-half of the FGM value.

Several authors [4,8,9] have addressed the exclusive nuclear transition in which the ^{12}C nucleus ($J^{\pi}=1^{+}$, $T=0$) remains intact, with one neutron changing to a proton, yielding the ground state of ^{12}N ($J^{\pi}=1^{+}$, $T=1$). Excited states of ^{12}N are particle unstable to ^{11}C$+p$. By selecting events with ^{12}N beta decay we are only sensitive to the ground state of ^{12}N. This transition to ^{12}N might provide evidence for induced second-class tensor and pseudoscalar currents in the weak interaction [10]. Induced currents are expected to be enhanced for ν_{μ} interactions as compared with ν_e since the former have a heavier lepton in the final state.

We describe the experimental details for these measurements in Sec. II. Our neutrino flux calculations are outlined in Sec. III and the event analysis is discussed in Sec. IV. The cross sections are obtained in Sec. V and the results discussed in Sec. VI.

II. EXPERIMENTAL DETAILS

A. Experimental layout

Our experiment was performed at the Los Alamos Meson Physics Facility (LAMPF) which delivers 800-MeV protons to a number of target locations. The experimental layout is shown in Fig. 1. The experiment was situated at a location that required the proton current to be shared with another beamline feeding the LAMPF Proton Storage Ring facility. We received an average of 20 μA of proton beam current delivered onto a water target in two running periods; the total integrated current was 5 C [11]. Among the particles emerging from the water target were pions that were allowed to decay in a tunnel 12 m long and 4 m in diameter, producing muon neutrinos and muons. A small fraction of the muons likewise decayed in the tunnel. Monte Carlo codes (described in Sec. III) were written to calculate the flux of muon and electron neutrinos (and antineutrinos) that

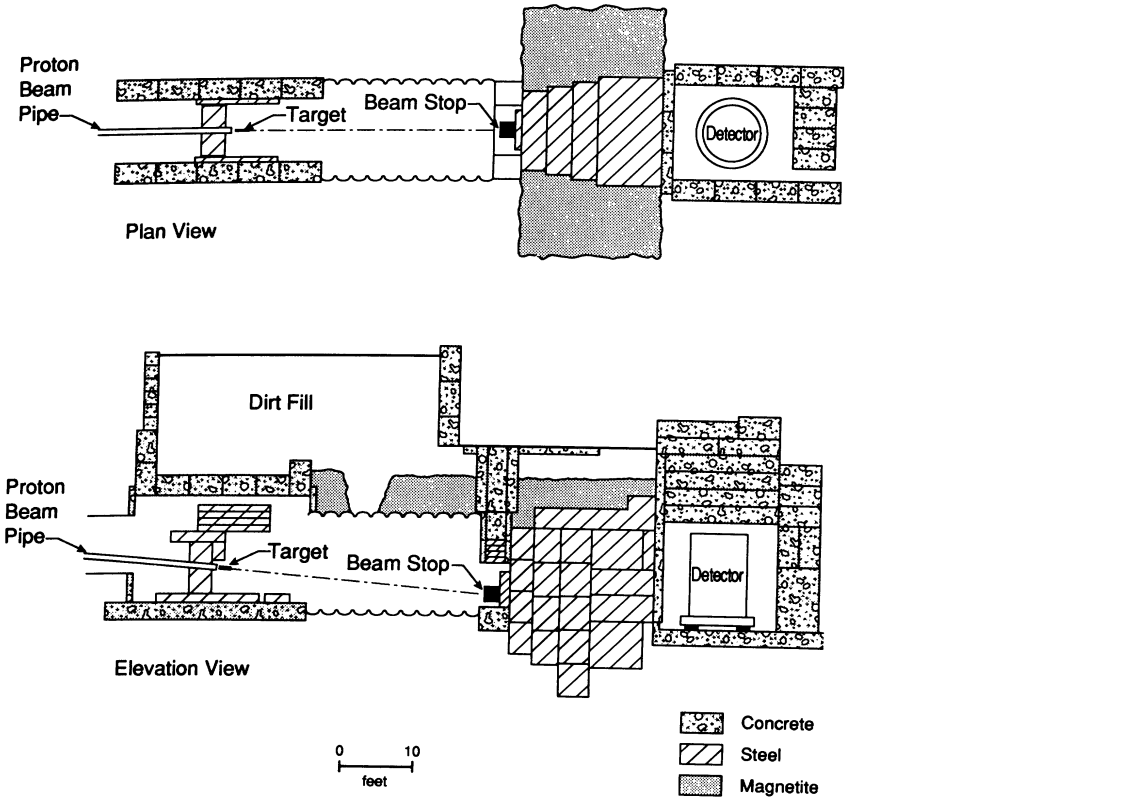

FIG. 1. The experimental setup is shown. Pions originating in the target decayed along the 12-m decay channel producing muon neutrinos. These struck the 5-ton scintillator detector which was set in a concrete bunker behind an 8-m-thick iron and magnetite shield.

would be observed in a detector placed downstream.

The center plane of the cylindrically shaped detector was placed 21 m from the entrance to the water pion production target. To minimize the cosmic-ray flux in the detector 4 m of concrete was placed over the detector and it was surrounded by 2 m of concrete on three sides. Immediately upstream of the detector was 8 m of steel to prevent hadrons and charged leptons generated in the target from entering the detector. Additional magnetite shielding was placed along the sides of the iron shield to further reduce the flux of scattered neutrons coming from reactions in the water target.

B. Proton beam line and target

The total LAMPF proton beam operated at 120 Hz of 800 to 1000-μs-long macropulses, each composed of 0.25-ns-long micropulses separated by 5 ns. As many as ten of these macropulses per second were deflected toward our pion-production target through a transport beamline [12]. The beamline monitors and pion-production target are discussed in detail elsewhere [13]. The incident proton current was measured by a toroid monitor placed just before the target and calibrated to 4% accuracy. A capacitive pickup device (CPU) sensitive to individual proton beam micropulses was used to provide fast (ns) timing relative to the proton beam.

The target was comprised of a 1-m-long stainless steel pipe, 25.4 mm in diameter and 0.25 mm in wall thickness, through which water was continuously circulated. The incident proton beam was focused to a spot of a few mm diameter and was sensed directly in the target by the change in water conductivity induced by the traversal of the beam. By the use of two conductivity monitors, one at the upstream end and the other at the downstream end of the target, we tracked the alignment of the incident beam throughout the experiment [13]. From the relative magnitudes of the signals on the two conductivity monitors we obtained a measure of the proton attenuation length through the water target of 87 ± 9 cm. This was consistent with a Monte Carlo calculation based on proton cross sections in water, and proton energy loss through the target, that yielded 94 cm.

C. Neutrino detector

The detector, shown in Fig. 2, was an upright aluminum cylinder filled with 4400 l of mineral-oil-based scintillator. The total active volume was 1.6 m in diameter and 2.14 m in height; there were 1.65×10^{29} carbon nuclei. To provide spatial segmentation, the detector was divided into 26 optically isolated vertical modules 2.14 m high and approximately 30 cm across. A 20-cm-diameter photomultiplier tube (PMT) was located at each end of the modules to collect the scintillation light from charged-particle trajectories within the modules; the effective energy threshold in each module was initially 10 MeV but was lowered to 3 MeV for most of the experiment. The detector cylinder was surrounded by two active veto shields, each consisting of an annular volume of liquid scintillator. A lead layer was located outside the outer active veto to convert incoming photons in order that they would be detected in the inner veto.

A scintillator hodoscope consisting of 14 vertical paddles (183 cm high$\times$15 cm wide$\times$5 cm thick) was fastened to the outside of the outermost veto shield. Each paddle used the timing from each end to determine the vertical position of charged cosmic-ray tracks. Eleven scintillator pairs on opposing sides of the detector were defined and used to track cosmic-ray muons through the detector modules for detector calibration purposes. During data taking, the hodoscope paddles were also included in the active cosmic-ray veto shield. The combined inefficiency of the veto shields was 8.3×10^{-6} for charged cosmic rays.

D. Data acquisition system

The LAMPF Q system [14] was used for data acquisition and provided high-speed data manipulation, online event analysis, and experiment monitoring. Hardware triggers were established in NIM hardware and, if satisfied, initiated the LAMPF trigger module. A pulse from the trigger module caused an MBD (microprogrammable branch driver) to determine from the trigger module which trigger was satisfied. The MBD then read the appropriate CAMAC modules for that trigger into

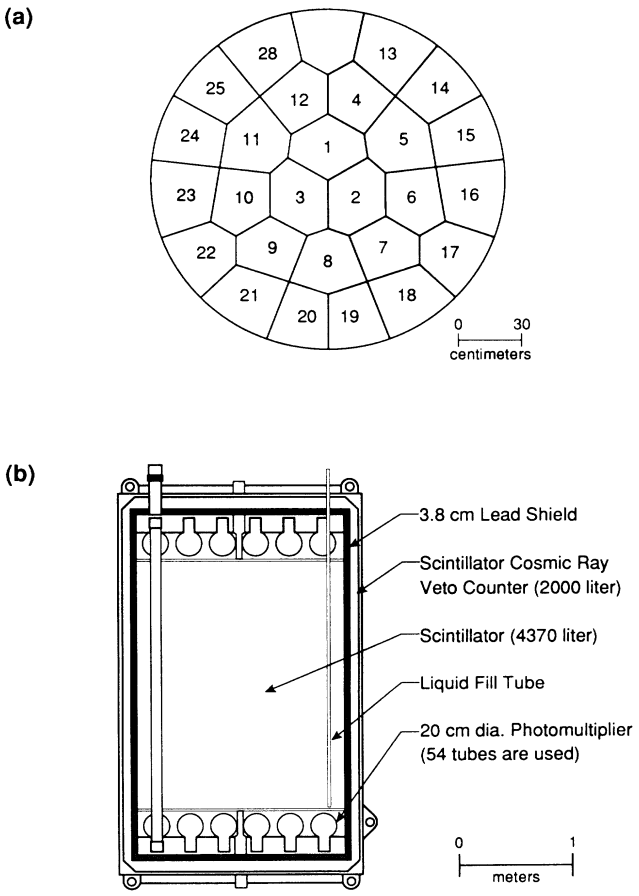

FIG. 2. (a) Neutrino detector top view indicating the 26 individual vertical modules. (b) Neutrino detector side view including the two active, liquid scintillator veto shields.

memory, followed by a transfer of these data to a computer. A substantial amount of online experiment monitoring and data analysis was done in the computer; data were also written to magnetic tape and analysis done offline.

E. Neutrino event triggers

In Fig. 3 the LAMPF beam structure, the beam gate B and the cosmic-ray gate G_C, are illustrated. In Fig. 4 the sequence of pulses and gates used to form the neutrino event trigger are displayed. The CPU was located immediately upstream of the pion-production target and was used to detect the arrival of the proton beam on the target. The CPU signal (delayed) stopped a TDC and thus measured the time of flight (TOF) of the incident particle.

Pulses from each of the detector's 52 PMT's were fed into analog-to-digital converters (ADC) and constant fraction discriminators (CFD); the CFD outputs of each pair of PMT's from each module fed mean timers. The 26 mean-timer outputs were "ORed" such that the earliest pulse P_μ during the beam gate corresponded to the initial time for a possible muon candidate from a neutrino interaction. The hardware trigger for a muon candidate was $T_\mu = P_\mu B G_\mu \bar{V}$, where $\bar{V}$ was a 5 μs veto gate triggered by a charged particle in the cosmic-ray veto shield. The presence of $\bar{V}$ removed false T_μ triggers caused by delayed electrons from cosmic-ray muons which stopped and decayed within 5 μs in the detector. Another trigger requirement, the periodic gate G_μ, suppressed triggers due to beam-associated neutrons (see Sec. II H).

Each time the trigger circuit T_μ was activated, a 20-μs gate G_e was opened. The mean-timer output pulse from

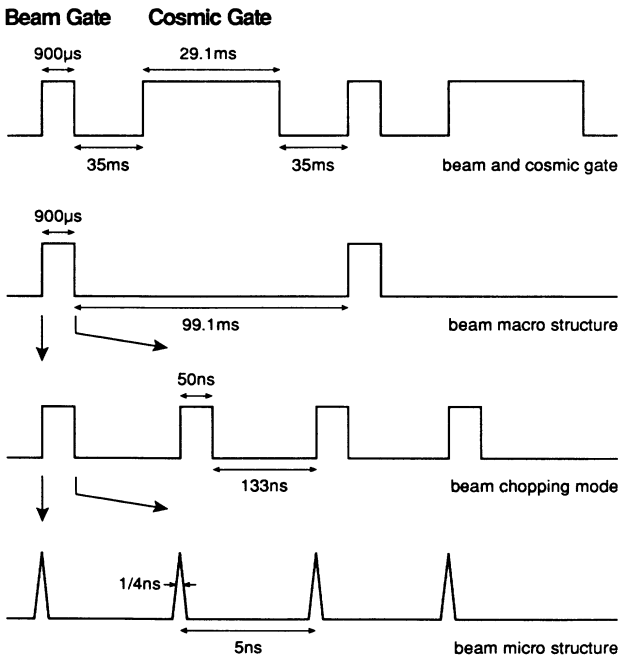

FIG. 3. Schematic view of the cosmic and beam gates with the beam structure.

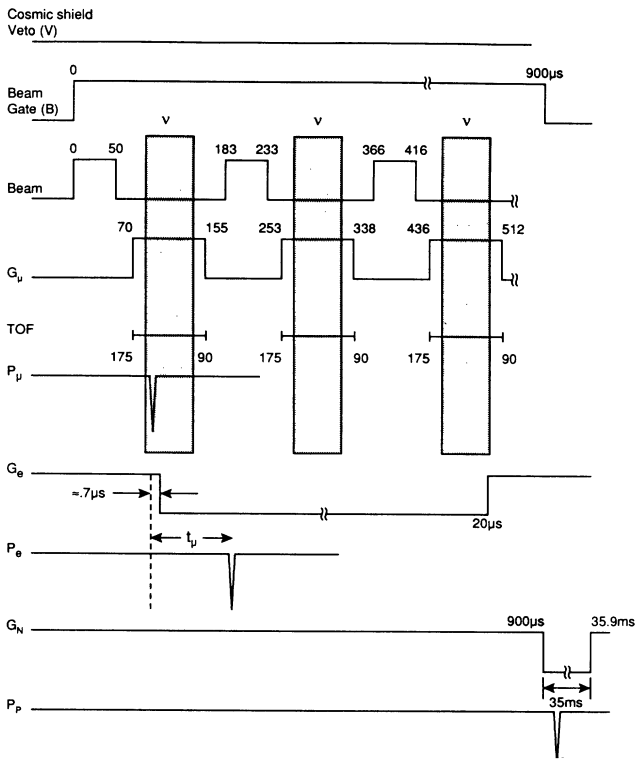

FIG. 4. Neutrino event gate sequence is shown. Note the breaks in the time axis and the changes in the time units.

any module(s) during this interval was recorded as a possible electron candidate from muon decay. The trigger for this electron was $T_e = P_e G_e$, where P_e is the output of the mean timer. Candidates for the inclusive reaction $^{12}\mathrm{C}(\nu_\mu,\mu^-)X$ were identified by the trigger $T_{\mathrm{inc}} = T_\mu T_e$.

To search for the exclusive reaction $^{12}\mathrm{C}(\nu_\mu,\mu^-)^{12}\mathrm{N}$(g.s.), a triple coincidence from prompt muon production, the electron from muon decay, and the positron from the ^{12}N decay were required. Since the mean lifetime of ^{12}N is 15.9 ms, a 35-ms gate G_N was opened at the conclusion of the beam gate B. A mean-timer pulse P_p observed during G_N was recorded as a possible positron from the ^{12}N decay. The signature for this exclusive event was then $T_{\mathrm{exc}} = T_\mu T_e T_N$, with $T_N = P_p G_N \bar{V}$.

The hardware triggers T_{inc} and T_{exc} were loose: the events triggered upon could occur anywhere in the detector and at this level were not required to be in spatial correlation. Offline analysis was used to isolate the true events and, as discussed below, the large sample of spatially uncorrelated events provided a means to study backgrounds.

F. Cosmic-ray triggers

To study cosmic-ray-induced background, to measure detector efficiencies, and to calibrate the detector, three cosmic-ray triggers were established during the time intervals between beam bursts. Cosmic-ray muons which stopped and decayed in the detector were identified by a trigger $T_{\mathrm{cc}} = P_\mu P_e V \bar{B}$, and were used to monitor the ener-

gy and timing calibrations (see also Sec. II G).

Those charged cosmic rays which passed completely through the detector were identified by a trigger $T_{\rm cth}=P_\mu P_{\rm H1}P_{\rm H2}V\bar{B}$, where the particle was required to pass through two hodoscope paddles, H1 and H2, on either side of the detector (see also Sec. II C).

Finally, to study cosmic-ray-induced events that might simulate a neutrino-induced signal, a trigger for neutral cosmic-ray particles was established that was essentially identical to T_μ, but occurred when there was no beam, i.e., $T_{\rm cn}=P_\mu G_c\bar{B}\bar{V}$. The G_e and G_N gates were also enabled following a $T_{\rm cn}$ trigger to look for signals which simulated the T_e and T_N triggers, respectively. The T_N signal in the cosmic-ray sample proved useful in identifying backgrounds from detector activation, as discussed later.

In addition, substantial amounts of offline cosmic-ray data were taken between data runs to study the performance of the detector and to measure the cosmic-ray veto efficiencies.

G. Detector calibration

Our experimental method required, for a charged particle traversing a portion of any of the 26 vertical modules in the detector, the determination for that module of the mean vertical (y) location of the track, of the energy lost by the particle, and of the relative time of the particle traversal. These physical quantities were determined from measurements of the time and amplitude of the pulses read out of the PMT's located at each end of the modules. High-energy cosmic-ray muons provided a nearly uniform illumination of the detector and were used for these calibration procedures.

Using the CFD times from the top (T_t) and bottom (T_b) phototube pulses, we obtained the y displacement of the track from the detector midplane, $y=(T_t-T_b+T_{\rm off})v_s$. Here, $T_{\rm off}$ corrects for a $y=0$ relative time offset for a module, and v_s is the speed of light in the scintillator. Timing measurements of cosmic-ray muons through the hodoscope, veto system, and central detector were used to measure $T_{\rm off}$ for each module. The signal velocity v_s and the spatial resolution σ_y, averaged over the entire detector, were 16 cm/ns and 12 cm, respectively.

The energy E deposited in a module by a charge particle was calculated from the ADC outputs of the top (A_t) and bottom (A_b) phototubes using $E=K_i(A_tA_b)^{0.5}$. In this manner, E was independent of the vertical position of the track in the module. The calibration constant K_i was determined separately for each module using minimum ionizing cosmic-ray muons satisfying the $T_{\rm cth}$ trigger, where the pairs of hodoscopes allowed the determination of the track length in each module. From these calibrations, we obtained $\sigma_E/E=12\%$ near 50 MeV. The hardware energy threshold for each module was 10 MeV during the initial run and 3 MeV during the subsequent run.

To obtain the relative timing between modules, hardware mean timers were used to measure the track arrival time $T_m=(T_t+T_b)/2$, which was independent of the vertical position of the track in the module. From the $T_{\rm cth}$ events, the relative timing between all modules was obtained to within 0.5 ns.

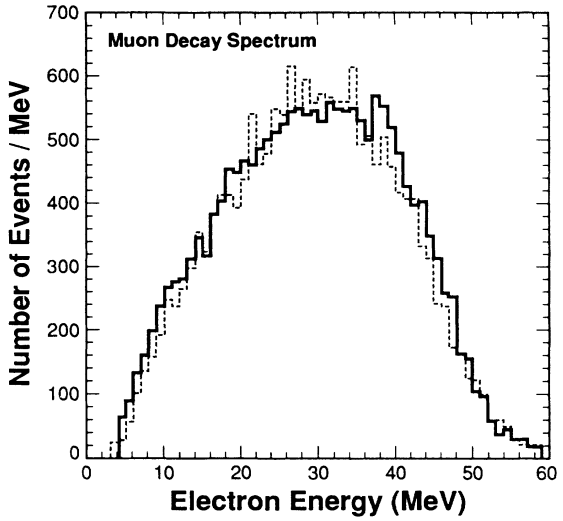

FIG. 5. The muon decay (Michel) spectrum is plotted for a sample of cosmic-ray muons that stopped in the detector. A Monte Carlo (MC764) calculation based on the EGS4 code, normalized to the total number of events, is given by the dashed line and shows good agreement with the data.

Cosmic-ray muon decays ($T_{\rm cc}$) were used to measure the energy deposited in the detector by the decay electrons, as shown in Fig. 5. The accompanying curve is from a Monte Carlo calculation (described in Sec. V) normalized to have the same number of events. The agreement confirms the energy calibration in the low-energy domain. In addition, the TDC output from these same events provided an absolute measurement of the stopped muon lifetime of $2.20\pm0.06\,\mu$s (Fig. 6), close to the value

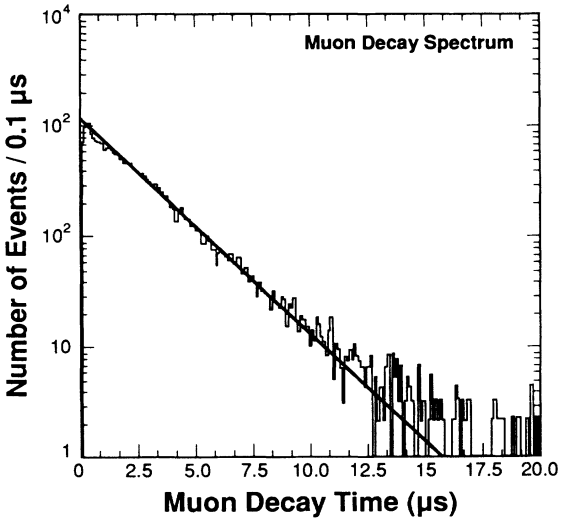

FIG. 6. The muon decay time spectrum is shown. The solid line is the decay curve corresponding to a muon lifetime of 2.20 μs.

2.12 μs expected from the combination of μ^+ (55%) and μ^- (45%) in the cosmic-ray flux [15]. The mean lifetime of μ^- in the scintillator, 2.026 μs, is taken from the measured value for carbon [16].

H. Proton beam chopping

The proton interactions in the water target generated a substantial number of neutrons. Almost all of the neutrons stopped in the iron shielding, but some scattered at large angles in the earth surrounding the shield and entered the neutrino detector. Even though their energies were much reduced, these neutrons were a nuisance because they produced knock-on proton recoils in the detector at a measured rate of 33 kHz and could have resulted in untenably large dead times in the experiment.

In order to reduce the effect of these neutrons, the TOF from the target to the detector was used to discriminate between prompt neutrino events and delayed neutron-induced backgrounds. However, the LAMPF beam macropulses were too long (about 1000 μs) to allow us to do this directly. Therefore, at the expense of average beam current, we chopped the macropulses at the injector to provide a pattern consisting of 50-ns regions of beam on, followed by 133-ns regions of beam off, as seen in Fig. 3 and in Fig. 4. This amounted to selecting 10 out of every 36 LAMPF micropulses. This pattern was chosen empirically to yield a TOF interval for neutrinos well separated from the bulk of the neutrons. Figure 7 shows the observed TOF in the detector with the chopped beam; the interval between arrows (a) and (b) shows the approximate 50-ns neutrino TOF region.

The energy spectrum of the muon candidate triggers, with the chopped beam in operation, is shown in Fig. 8.

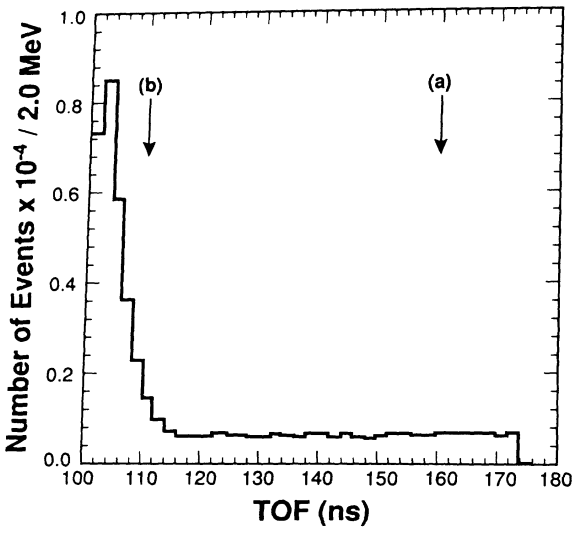

FIG. 7. Spectrum of T_{inc} trigger times (TOF) relative to the leading edge of the capacitive pickup (CPU) for the proton beam spill onto the pion-production target. Longer time differences correspond to smaller TOF numbers. The arrows (a) and (b) delineate the neutrino arrival region. Evidence of beam-related fast neutrons is apparent in the excess of late-arriving events in the interval TOF < 110 ns.

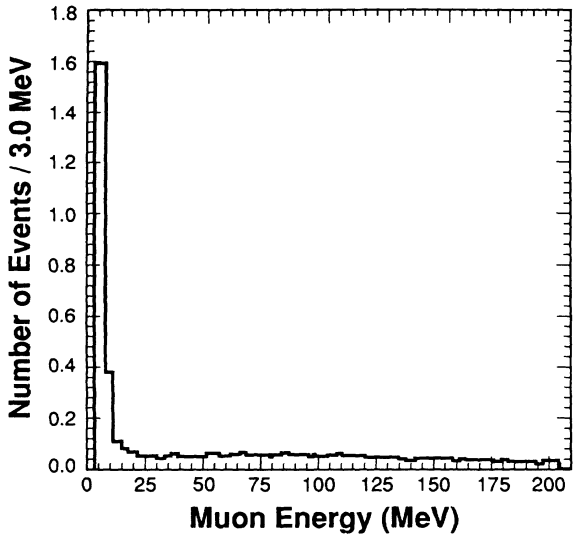

FIG. 8. Energy spectrum of muon candidate triggers with the chopped proton beam. The peak results from accidental coincidence between low-energy signals in the muon interval and low-energy neutron signals in the decay electron gate.

Assuming that the observed energy spectrum results predominantly from proton recoils in the detector, we found that the average neutron energies were less than 20 MeV, which is expected for neutrons that scatter at large angles in the earth surrounding the iron shield. With the unchopped beam we could look for the presence of high-energy neutrons; from the maximum observed energy of the proton recoils we found no evidence for copious numbers of scattered neutrons having sufficient energy (> 400 MeV) to produce a pion in the detector. These could have resulted in a background of muons in the experiment if the decay of the pion were missed.

To reduce the dead time in the detector caused by arrival of beam-associated neutrons, we introduced the muon gate G_μ shown in Fig. 4. G_μ gated off the muon trigger during the 98-ns periods when most of the neutrons arrived. The muon trigger was cycled on again for 85 ns in order to include both the 50-ns-long neutrino TOF region and a control region on either side when no neutrinos were expected. This allowed us to monitor any residual neutron effects in the detector. The effect of G_μ was to reduce the peak trigger rate of 33 kHz to a manageable rate of 1.6 Hz, thereby producing little dead time in the experiment. However, neutrons interacting in the active cosmic-ray shield did turn off the detector and produce an appreciable dead time. This effect was measured to be 15.5% in G_μ and 8.8% in the electron gate G_e; it dominated the dead time in the experiment.

While G_μ eliminated the direct neutron-induced backgrounds involving neutron scattering, there was a small activation rate in the detector resulting from (n,p) knock-out reactions such as $^{12}\text{C}(n,p)^{12}\text{B}$, followed by the ^{12}B beta decay. The resultant beta decays had lifetimes near 15 ms observed in the T_N gate. They are expected to have a fairly constant rate during the muon and decay electron gates, thus producing a background dispersed

randomly throughout the detector. The energy deposited by the beta decay was small, less than 15 MeV, so that backgrounds from this activation would be greatest at low energies.

The electron gate G_e was not modulated in the same manner as was the muon gate. However, the time of any signal in the electron interval relative to the CPU (TOF_e) was recorded. This information was used later to provide a clean sample of events with low muon kinetic energy, where backgrounds from activation were greatest (see Sec. IV A).

The start of the neutrino TOF interval in the detector was calibrated relative to the proton beam on target by using two small scintillator counters, arranged one behind the other, to measure coincidences of particles traversing them. These were placed in the decay channel 8 m downstream of the water target. With the incident proton beam chopped to intervals of 1-ns duration every μs, signals were identified from the scintillation counters that corresponded to photons and pions generated in the target, and their TOF in the counters was measured relative to the CPU. The counters were then placed over the neutrino detector. With the electronics and cable lengths left unchanged, cosmic-ray coincidences were observed between the counter pair and the neutrino detector. In this way the detector electronics timing was calculated relative to beam protons that passed through the CPU. Using the flight time from the CPU to the target for protons, and the distance from the target to the center of the detector, the earliest arrival time for neutrinos was determined. A second estimate of the neutrino TOF interval was made by measuring the signal cable lengths and electronics delays. The two methods were consistent to within 5 ns.

During the experiment, the signal observed by the CPU for each micropulse was proportional to the beam current; this current depended on the accelerator operating conditions. The electronic circuit from the CPU had a threshold to sense if micropulses were present, and this had an efficiency that depended on the pulse height in the CPU. The beam-chopping device at the source end of the LAMPF accelerator was found to have a rise time that often caused a reduced intensity for the first one or two micropulses out of the ten that were selected for the neutrino beam. This produced an observed jitter of about 10 ns in the start of the neutrino TOF region. (We discuss this in detail in Sec. IV A.)

III. NEUTRINO FLUX

Three independent Monte Carlo codes (MC) were written to calculate the neutrino flux in the detector [17–19]. The general features of these codes are described here. Since the experiment was sensitive to neutrinos with energies $E_\nu > 100$ MeV, the codes treated the decay in flight of pions and muons; decay at rest was ignored.

In the MC programs, 800-MeV protons from LAMPF were followed through our pion-production target. The target was a cylinder of water 1 m long and 2.5 cm in diameter. Since no *in situ* measurements of the pion production from proton interactions in our target were possible, the MC codes relied on previously measured energy-dependent differential cross sections for pion production [20] and a MC model of the proton interactions in the target to obtain the pions emerging from the target.

Energy-dependent cross sections for proton elastic and inelastic interactions [21], with hydrogen and with oxygen, were used in the simulations. If the proton produced a pion, the measured energy-dependent pion differential cross sections were interpolated to find the momentum vector for the pion produced. While the three MC codes used the same published doubly differential cross sections for pion production, the parametrization of these cross sections for interpolation purposes differed between them. A main limitation in the precision of the flux calculation for each code was the extrapolations required, because there is little cross section data for pions produced at small angles with respect to the incident proton.

In each MC the positive and negative pions produced in the target were followed to the target perimeter, taking account of energy loss, absorption losses, scattering, and decays. Once the pions emerged from the target, they were followed until they decayed or encountered the decay channel boundary. After a decay both the muon and the muon neutrino were followed, the former until it decayed or encountered the decay channel boundary, the latter until it was determined whether it would intersect the vertical midplane of the detector. Likewise, the electron neutrinos that come from muon decay were followed to see if they intersected the midplane of the detector. In this fashion, we were able to calculate the energy-dependent flux of neutrinos in the detector per incident proton.

In Fig. 9, we show the normalized ν_μ and $\bar{\nu}_\mu$ fluxes above 100 MeV. The flux of ν_e was about 2.4×10^{-3} that of the ν_μ flux and was therefore neglected. Additional details of the calculations can be found in Refs. [17–19].

The uncertainty associated with the flux values is estimated to be 18%. Contributions to this uncertainty consist of the error in the proton interaction cross section

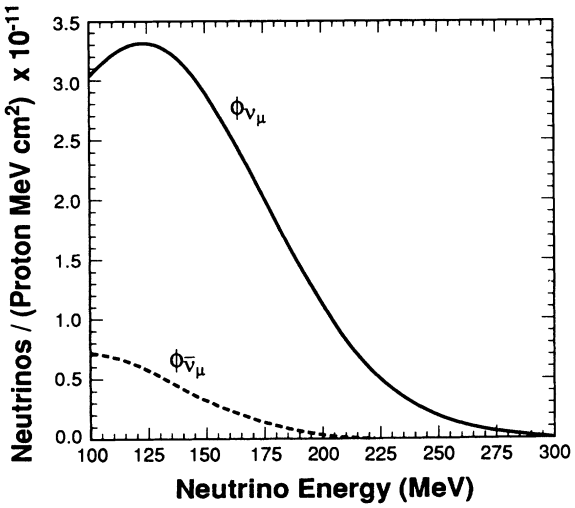

FIG. 9. Calculated ν_μ and $\bar{\nu}_\mu$ flux in the detector from pion and muon decays in the decay channel.

in water and the errors in the published pion production and absorption cross sections and their extrapolation (15%), and the deviations in the flux calculations between the different Monte Carlo codes (9.4%). The total muon neutrino flux, integrated from 123.2 (muon-production threshold on carbon) to 300 MeV, is $(2.0\pm0.4)\times10^{-9}\nu_\mu$ cm^{-2} proton^{-1}.

IV. EVENT ANALYSIS

Beam-on data were collected in two running periods. As seen in Table I, the combined data contain 847 429 $T_{\rm inc}$ triggers that were candidate events for the inclusive reaction $^{12}C(\nu_\mu,\mu^-)X$. In addition, as described in Sec. II, we also tagged a subset of $T_{\rm inc}$ triggers that were consistent with the exclusive ^{12}N(g.s.) final state. In this section we describe the event selection processes for both channels.

A. Inclusive charged-current process

To isolate the true $^{12}C(\nu_\mu,\mu^-)X$ events from among the 847 429 candidates, a series of cuts were applied. At the same time, the identical cuts were applied to a large control sample of stopped cosmic-ray muons whose trigger $T_{\rm cc}$ is described in Sec. II F. This latter effort permitted us to estimate, in a model-independent manner, the expected pass-through rate for $^{12}C(\nu_\mu,\mu^-)X$ events for each cut applied to the data. These results are also shown in Table I and are discussed in this section.

The 847 429 $T_{\rm inc}$ triggers were obtained using the 85-ns-wide TOF window, allowing the observation of the tail of the slow neutrons arriving at the detector after the arrival of the neutrinos. From the energy distribution of the muon candidates, evidence is found for the arrival of fast beam-associated neutrons for TOF <110 ns; by applying a more restrictive cut from 100 ns (late arrivals) to 160 ns (earliest arrivals) as seen on Fig. 7, nearly 53% of the background $T_{\rm inc}$ triggers was removed.

The vast majority of the remaining candidates were expected to be spurious $T_{\rm inc}$ triggers caused by a low-energy pulse in the muon gate G_μ (due to decay electrons from activated material in the detector) followed by a random pulse in the electron gate G_e (generally the result of a proton recoil from a beam-associated neutron-induced interaction). Neutron-induced pulses in the electron gate were possible since, in contrast to the muon gate, the detector was not blanked during the neutron part of the TOF interval. Furthermore, no requirement was made in the hardware trigger based upon the spatial proximity of the muon and electron pulse.

From the control sample of stopped cosmic-ray muons it was determined that 95% of the decay electron signals occurred in the same module within ±40 cm of the parent muon along the vertical height of the module. When these cuts were applied to the data sample, the number of triggers was reduced by a factor of 46.

A cut on the maximum time difference from module to module in the decay electron time interval served to further reduce the number of slow proton recoils crossing module boundaries. This decreased the data sample by a factor of 2.2 and the control sample by 7%. In events with multiple module hits in the decay electron interval, the requirement that the hits be spatially contiguous cut out an additional 16% of our control sample but reduced the number of charged-current candidates by a factor of 1.6.

To further remove low-energy, neutron-induced proton recoils in the decay gate G_e, a threshold energy cut of 15 MeV was imposed on pulses in the electron gate. While this reduced the candidate sample by a factor of 13.7, the additional loss of real events was only 10%, as determined from the energy spectrum of Michel electrons in the large sample of stopped cosmic-ray muons.

The 1-ns timing resolution between modules in some cases could be used to determine the direction of the

TABLE I. Effect of restrictions on the sample of inclusive and exclusive event candidates. See the text for explanation.

Constraint	Candidates surviving	Signal surviving (%)
Total muon triggers	847 429	
Neutrino TOF interval	445 368	100
Muon and electron signal spatial correlation	9611	95
Muon decay: module-to-module TOF <5 ns	4455	93
Spatial continuity of muon decay track	2777	84
Muon decay electron energy >15 MeV	202	90
Decay at wrong end of muon track	132	100
Fiducial volume	108	99
Total weighted inclusive events	142.0 (107.2)[a]	
Total weighted exclusive ^{12}N events	4.6 (3.8)	
Total efficiency for inclusive signal		66
Total efficiency for exclusive signal		28

[a]The values in parentheses are after random background subtraction.

muon track and thereby reject candidates where the contiguous modules in the decay electron gate appeared at the wrong end of the muon track. A further reduction in the candidate sample of 1.5 was achieved using this cut, with no reduction in the control sample.

Finally, a cut was applied on events near the vertical boundaries of the detector to eliminate possible interactions occurring in the Plexiglass windows. This reduced the number of candidate events by 18%, while having only a 1% effect on the expected signal.

The above procedure yielded a total raw-event sample of 108 charged-current candidates, corresponding to a net survival efficiency in our control sample of 66.0% due to our cuts (see Table I). Employing graphical event displays, we examined the data from a random sample of 2000 $T_{\rm inc}$ events on an event-by-event basis. This examination confirmed the assumption that these cuts were being applied in a uniform, unbiased fashion.

For the events with prompt energies less than 10 MeV the random background expected would be higher than for the rest of the data sample due to neutron-induced activation. The strategy employed was to apply a timing cut (TOF_e) in the decay electron interval relative to the CPU as described in Sec. II. Such a cut eliminated the region in this interval where neutron-induced knock-on protons dominated. This cut eliminated one-half of the electron interval by introducing a series of equally spaced 92-ns "holes" across the entire electron gate. Therefore, for the surviving events we obtained the real number of events, in this low-energy region, by weighting them by a factor of 2. When the TOF_e cut was applied to all $T_{\rm inc}$ triggers with less than 10 MeV in the muon gate, 30 events remained in this sample; these were then weighted by the factor of 2 to obtain 60 events for the corrected number.

An additional correction was applied to these data. The first one-third of the data collected were obtained with an energy threshold per module of 10 MeV, as compared to the threshold of 3 MeV for the bulk of the data. To correct for the resultant 23% lower detection efficiency, the 17 surviving candidates from the earlier period were weighted accordingly to produce 21 events. These corrections yield a final sample of 142 weighted neutrino charged-current candidate events.

A histogram of the decay time of the 142 weighted $^{12}\mathrm{C}(\nu_\mu,\mu^-)X$ candidates that survived our cuts is shown in Fig. 10. A fraction of the first microsecond (approximately 0.7 μs) in the decay electron interval was blanked out in the hardware to prevent the long PMT pulse widths from the muon interval from extending into the decay electron region as shown in Fig. 4. In the offline analysis all events with a decay time less than 1.0 μs were ignored. Therefore, since none of the previous cuts biased muon decay times above 1.0 μs, we used this histogram to search for evidence of additional backgrounds which remained in this sample. The neutrino signal is expected to appear within several muon lifetimes; the time interval up to 7 μs was selected. However, events at larger lifetimes, where backgrounds would dominate, were observed. By applying the same cut analysis to the large sample of "beam-off" cosmic-ray triggers, $T_{\rm cn}$, it

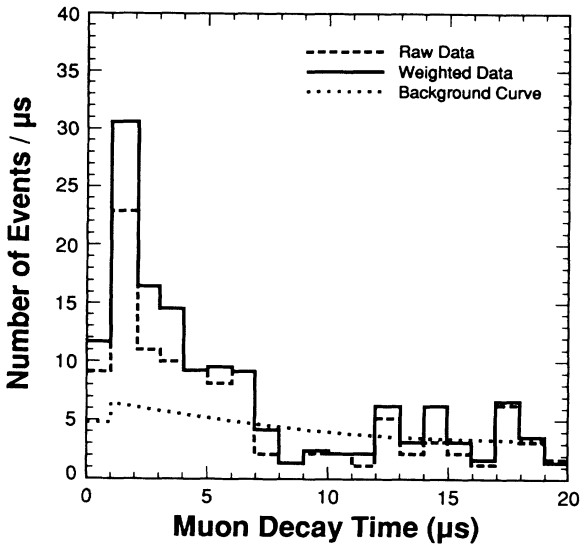

FIG. 10. Time of T_e trigger (decay electron) relative to $T_{\rm inc}$ trigger (muon) corresponding to the lifetime of the muons. The dashed line is the raw data after applying all cuts; the solid line is that same data after applying weights; the dotted line is the random time spectrum of background events.

was possible to deduce that a completely negligible number of the events in Fig. 10 could be ascribed to cosmic rays. Therefore, the remaining background was attributed to randomly distributed activation-induced events, and the following method was devised to remove them.

In general the activation-induced background events have the muon pulse and electron pulse spatially uncorrelated. Thus the previous requirement that these pulses be spatially connected removed most of those background events. To remove the remaining background we utilize the decay time of $T_{\rm inc}$ triggers in which the pulses are chosen to be spatially uncorrelated. Weighting these events by the appropriate combinatorics associated with 26 modules in our detector, both the level and the time dependence of the accidental background were obtained as shown in Fig. 10. There are no free parameters in this estimation. It is evident that this background curve compares favorably with the observed charged-current candidates for long decay times, where the backgrounds are expected to dominate, and this gives evidence that the last major source of background is removed. In Fig. 11, the remaining signal after subtracting this background is shown. The sample of events used to estimate the activation-induced backgrounds was two orders of magnitude larger than the 142 neutrino candidates that had survived our cuts, thus yielding a precise value for the level of background remaining in the signal region.

A one-parameter fit to the remaining signal ($1<t_\mu<7$ μs) with a fixed muon lifetime of 2.026 μs is also shown and is a good fit ($\chi^2_{\rm DOF}=0.35$) to the data over the entire electron gate interval. As mentioned before, a muon lifetime of 2.026 μs is appropriate for negative muons after taking into account absorption in the scintillator. This yields a zero-time intercept of $\alpha_0=46.4\pm7.8$ events/μs.

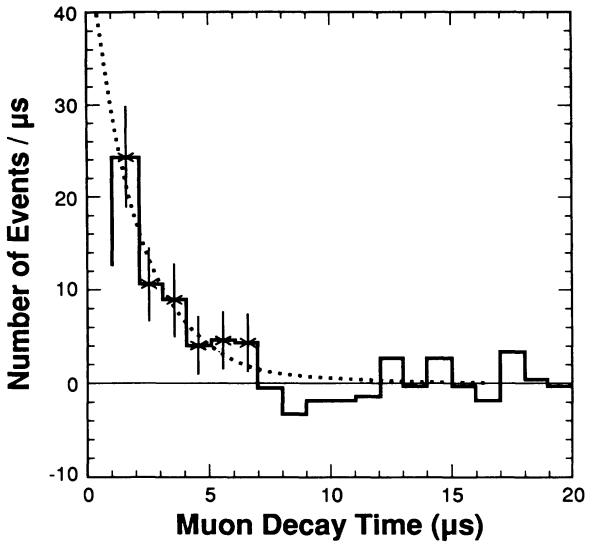

FIG. 11. Lifetime of ν_μ-induced events after background subtraction (Fig. 10). The smooth curve is fitted to the data for a lifetime of 2.023 μs. The spectrum beyond 7 μs is consistent with zero.

As a check of this procedure, a two-parameter fit to this same region yielded an intercept of 43.2 ± 2.2 events/μs and a lifetime of 2.15 ± 0.08 μs with $\chi^2_{\rm DOF}=0.43$.

As noted above, the earliest arriving neutrinos are expected to appear at 160 ns in the TOF spectrum (Fig. 7) and to extend to 110 ns, corresponding to the 50-ns-wide proton beam pulse. The preceding analysis, summarized in Table I, used this TOF region to produce the 142 charged-current candidates. However, a jitter of about 10 ns in the neutrino TOF region, due to the response of the CPU, was observed as described in Sec. II H. In the absence of this pickoff jitter, the weighted neutrino charged-current candidates are expected to be evenly distributed over the 50-ns-wide neutrino window. The effect of jitter is a depletion of neutrino events in the region 140–160 ns, and a shift of neutrino events into the TOF region <110 ns; hence, these events would not have been included in the above analysis.

A correction is now applied for the jitter in the neutrino TOF window. The detailed time structure of the jitter along the TOF axis in the earlier and later TOF regions is unknown; however, the neutrino TOF region is 50 ns wide and the neutrino yield over this 50 ns is flat, based upon the shape of the proton spill on the production target. From the time dependence of the candidate events in the region $110<\text{TOF}<160$ ns, it can be estimated that 13% of the neutrino-induced events had spilled out into the region TOF <110 ns; hence, the event sample is multiplied by a correction factor 1.14 ± 0.06. Since all events in the region $110<\text{TOF}<160$ ns were used in the muon lifetime plot, the number of $^{12}\text{C}(\nu_\mu,\mu^-)X$ events is calculated to be

$$N_{\rm inc}=\alpha_0(2.026\ \mu\text{s})(1.14)\ . \tag{1}$$

In this equation α_0 is the fitted intercept from Fig. 11, and the factor of (1.14) is the correction described above. Inserting the measured values into this equation, $N_{\rm inc}=107.2\pm19.0$ events from the inclusive reaction $^{12}\text{C}(\nu_\mu,\mu^-)X$ are obtained.

B. Exclusive charged-current process

As pointed out in Sec. II, the experimental signature for the exclusive channel in which ^{12}N remains in the ground state is a three-step process $T_{\rm exc}=T_\mu T_e T_N$, wherein these events are a subset of the inclusive event sample $T_{\rm inc}=T_\mu T_e$ analyzed above. Only four events from among these in Fig. 10 had a positron candidate from the ^{12}N decay in the 35-ms G_N gate following the LAMPF beam spill. These events were required to have the module(s) in which the positron was detected to be spatially associated with the module containing the muon. Each event was observed to have a ^{12}N decay energy less than 20 MeV, consistent with the positron endpoint energy of 16.3 MeV. None of these four events had muon lifetimes greater than 7 μs. One of these events came from the earlier run; after applying weighting factors for this event in the manner described in Sec. IV A, 4.6 weighted events remained.

An analysis similar to that above was performed on a large sample of $T_{\rm exc}$ triggers for which the muon, electron, and positron were spatially disassociated to estimate the expected random background in our ^{12}N sample from neutron-induced activation. This analysis produced an expected background of 0.8 event with a small uncertainty, thus giving us a signal of 3.8 ± 1.4 events. The uncertainty was assigned from Poisson statistics.

V. CROSS SECTIONS

To express the results in terms of interaction cross sections, the number of events must be normalized to the expected number of muon neutrinos in the detector, and these events must be corrected for several detector inefficiencies, other than the weighting factors introduced above, and for beam-induced backgrounds.

A. Inclusive cross section $^{12}\text{C}(\nu_\mu,\mu^-)X$

A loss of events occurred when the muon signal was below the trigger threshold. Light attenuation in the liquid scintillator made the trigger threshold dependent on the vertical position y along the module. Requiring that both PMT's fired at each end of the module for a legitimate trigger resulted in a loss when events occurred close to one or the other end of the module. As the neutrino events were distributed evenly in y, this loss was determined to be 10% from the falloff of the vertical distribution of the data.

In order to better understand various inefficiencies and backgrounds in our detector system, a Monte Carlo program MC-764 based upon the EGS4 shower code [22] was employed to construct ν_μ-induced charged-current events in our detector. The modular detector geometry and the measured spatial, energy, and timing resolutions were put into the code. As mentioned earlier, this Monte Carlo program was used to predict the Michel electron energy

distribution from stopped muons that decayed in the detector. As a check the predicted spectrum was compared with the corresponding measured spectrum from cosmic rays as shown in Fig. 5. The agreement is good across the entire energy range.

To study the detector response to muon from charged-current ν_μ interactions in our detector, the FGM [3] was used with appropriate Coulomb corrections, and with the neutrino flux shape from Sec. III, to produce the muon kinetic-energy distribution. Since the corrections to the results as described below were small, the dependence of the corrections on the assumed model and the flux shape is likewise small.

From the MC-764 code it was determined [23] that 2% of the ν_μ-induced muons in the detector were lost due to capture in the scintillator and in the aluminum walls of the detector prior to decay. In addition, approximately 1% of the muons went undetected since their energy was below the 3-MeV absolute energy threshold per module. Using FGM cross sections for aluminum and lead in the MC-764 program, we estimated that 21% of the detected ν_μ events in our sample actually occurred off the aluminum and lead in the detector. The total event rate was corrected both to remove this background and to account for the small losses in ν_μ-induced events.

While the neutrino energy was too low to allow charged-current ν_μ interactions off free protons (a positive pion must be produced along with the negative muon), $\bar{\nu}_\mu$ interactions with free protons are possible, resulting in a μ^+ in the final state. The neutrino flux calculation programs (Sec. III) gave an estimate of a 14% $\bar{\nu}_\mu$ contaminate in our ν_μ beam. From the $\bar{\nu}_\mu$ to ν_μ ratios for (a) the relative nucleon charged-current cross sections (0.333), (b) the cross-section weighted targets (2.08), (c) the μ^+ to μ^- capture (1.11), and (d) the calculated neutrino flux (0.16), it is estimated that 11% of our charged-current events were $\bar{\nu}_\mu$-induced events.

The number of protons delivered by LAMPF during the experiment was measured by a toroid just upstream of the target. The toroid was scaled only when the detector was active and recorded a total of $(2.60\pm0.14)\times10^{19}$ protons on target over the course of the experiment. Using the number of $N_{\rm inc}$ charged-current events from Sec. IV A (107 ± 19), the neutrino flux from Sec. III [$(2.0\pm0.4)\times10^{-9}\nu_\mu$ cm$^{-2}p^{-1}$], the number of protons on target, the efficiency of 66% from Sec. IV, the number of carbon nuclei in the detector (1.65×10^{29}), and a factor of 0.81 for the corrections described above, our inclusive charged-current cross section is $(15.9\pm2.6\pm3.7)\times10^{-39}$ cm^2. The first error is statistical. The second is an estimate of the systematic errors which include a 6% uncertainty in the number of protons delivered, an 18% uncertainty for the flux calculation, and an estimated 10% each for the efficiency and for corrections applied to the data, all added in quadrature.

B. Exclusive cross section ^{12}C(ν_μ,μ^-)^{12}N(g.s.)

Because the event signature for the exclusive transition involves a coincidence with the ^{12}N decay, there is no correction needed for ν_μ reactions on aluminum and lead, and the $\bar{\nu}_\mu$ background is treated differently as described below. However, several new corrections need to be made to the exclusive event sample. Based on the EGS4 Monte Carlo described in Sec. IV, the efficiency of the detector for the ^{12}N decay is estimated to be 58%. The spatial cuts on the ^{12}N decay had an efficiency of 85%, and the ^{12}N lifetime interval efficiency was 86%. The combined efficiency for the additional requirement of the T_N signature is then 42%. None of the applied cuts should bias the muon decay time. All four ^{12}N candidate events have muon decay times less than 7 μs.

A background correction to be applied to these data is the event rate due to $\bar{\nu}_\mu$ interactions yielding ^{12}B nuclei that can mimic the ^{12}N events. From particle-hole model calculations [8] and from the 14% $\bar{\nu}_\mu$ component of the neutrino beam, it is calculated that 0.2 $\bar{\nu}_\mu$ events contaminate the sample and must be subtracted. The exclusive reaction total of 3.8 events, from Sec. IV B, is then reduced to 3.6 events.

From the resulting sample of 3.6 events, the flux values from Sec. III, and the application of a combined efficiency and correction factor of 0.24, a cross section for the exclusive reaction ^{12}C(ν_μ,μ^-)^{12}N(g.s.) of $(1.7\pm0.8\pm0.3)\times10^{-39}$ cm^2 is obtained. The first error is statistical while the second is systematic owing primarily to the neutrino flux calculation. This transition to the ^{12}N(g.s.) represents 11 ± 5 % of the total carbon event rate.

VI. RESULTS AND DISCUSSION

To compare the measurements with the FGM of Ref. [3], the binding energy for carbon is taken to be 25 MeV and the Fermi momentum to be 221 MeV/c. These values were derived from electron-scattering data [24] that have been successfully described by the FGM. Because there are low-energy muons in the final state, the cross section of Ref. [3] is multiplied by a factor to correct for the Coulomb interaction between the outgoing negative muon and the nuclear charge. This factor enhances the cross section [25] in a manner similar to the Sommerfeld factor in nuclear beta decay and has been required to explain pion-photoproduction experiments [25,26] near threshold. This multiplicative factor S is given by

$$S=2\pi\eta(e^{2\pi\eta}-1)^{-1}\ . \tag{2}$$

Here, $\eta=Z\alpha\beta^{-1}$, where Z is the atomic number, α is the fine-structure constant, β is the speed of the lepton, and η is negative for an outgoing negative lepton. The full factor S is appropriate when the nucleus remains intact after the interaction. In this experiment, the nucleus could break up in many events causing some nuclear charge to leak away. Therefore, the Coulomb correction as applied ($\sim15\%$) may be an overestimate. The resultant cross section, with the Coulomb correction, is shown in Fig. 12.

Folding the Coulomb-corrected FGM cross section as a function of energy with the neutrino flux shape enabled a calculation of a mean neutrino interaction energy of 202 MeV over the energy interval from the muon thresh-

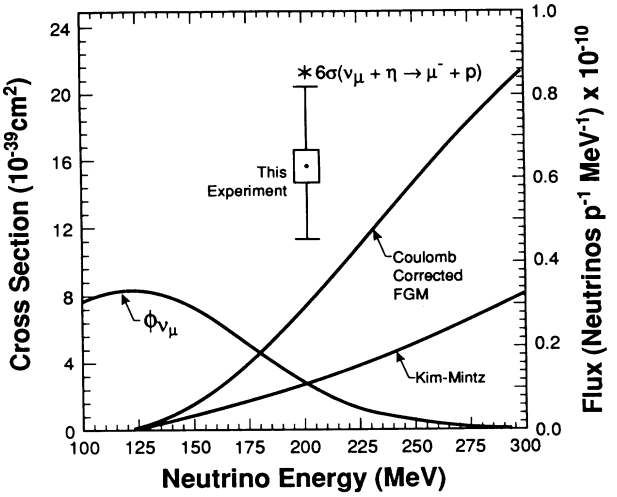

FIG. 12. Our measured inclusive muon-neutrino carbon cross-section result is given by the data point. Folding the Fermi-gas model (FGM) cross section [3] with our neutrino flux spectrum, we calculate a mean neutrino interaction energy of 202 MeV for our flux-weighted cross-section measurement. Theoretical predictions for the cross section are given for the Coulomb-corrected FGM (solid line) and for the calculation of Ref. [7] (dashed line). The free nucleon cross section $n(\nu_\mu,\mu^-)p$ is shown, for comparison, as the single point.

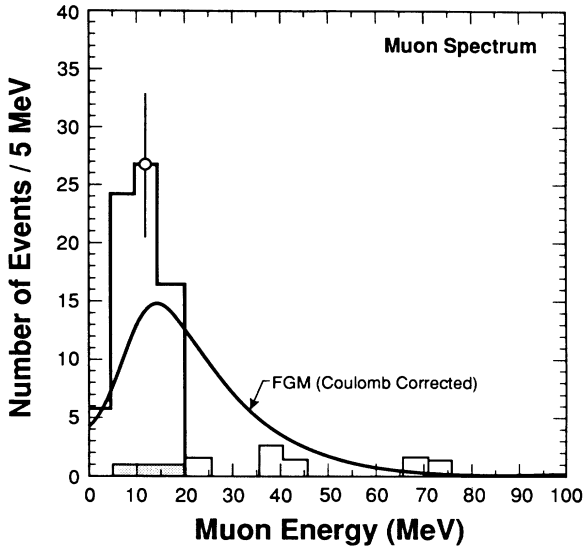

FIG. 13. This histogram is our measured spectrum of muon energies, with random backgrounds subtracted. The curve was generated from the FGM and was normalized to the total number of measured events in the inclusive reaction channel. Events with a ^{12}N beta decay in coincidence are shown as cross hatched.

old to 300 MeV. The measured $^{12}C(\nu_\mu,\mu^-)X$ inclusive cross-section value, 15.9×10^{-39} cm^2, is plotted in Fig. 12. At the average neutrino interaction energy $E_{\nu_\mu}=202$ MeV, the measured cross section is over one standard deviation larger than the Coulomb-corrected FGM prediction, and over one standard deviation smaller than the free neutron cross section.

Further comparison can be made with the earlier literature. The present result is over two standard deviations larger than the values suggested in Ref. [7] and those obtained in a previous measurement [6]. Also, the value 1.5×10^{-39} cm^2 quoted in Ref. [4], where only nuclear transitions to the $T=1$ bound and unbound states of ^{12}N are taken into account, is in disagreement with the present measurement of the inclusive cross section.

The measurement of the muon kinetic energy, which is shown in Fig. 13 after subtraction of the activation-induced background, is a more severe test of the FGM calculation. When phase space is considered for the neutrino-nucleus interaction [3], the cross section vanishes as the muon kinetic energy goes to zero. Theoretically, the cross section does not vanish [25], but is expected to have a finite value due to the final-state Coulomb interaction. After taking the Coulomb interaction into account, the FGM prediction of the muon kinetic-energy distribution, normalized to the total number of events, is shown in Fig. 13. The data in the first two bins have been corrected to take into account the losses due to the energy thresholds as discussed above: a 10% correction for the loss in the vertical distribution and a 1% correction for the absolute energy threshold. The relative detection efficiency for observing muons in the detector is basically independent of energy above the threshold of 10 MeV. However, there is a few percent effect at higher muon energy due to muon events near the detector wall that escaped before decay. This inefficiency was included in the MC-764 Monte Carlo detector simulation (Sec. V A), which was used to calculate the FGM muon energy spectrum in Fig. 13. The present measurement shows a marked depletion of events at high muon energies, and a corresponding increase of events at low energies, compared to the FGM prediction. Because the FGM reflects the average behavior of the interaction, and does not contain mechanisms for the transfer of energy to specific nuclear degrees of freedom, it is not expected to account in detail for the relative strengths of highly excited nuclear states. Consequently, it is not surprising that significant differences between the FGM and this measured muon kinetic-energy distribution [27] exist.

The cross-hatched events in Fig. 13 show the muon energy distribution of the observed events, after background subtraction, with a ^{12}N beta decay in the final state. The measured value for the production of the ^{12}N ground state, $(1.7\pm0.9)\times10^{-39}$ cm^2, albeit with a large uncertainty, is considerably higher than the predictions of 0.8×10^{-40} cm^2 in Refs. [2,8] and 0.7×10^{-40} cm^2 in Ref. [4]. Mintz and Pourkaviani [28] point out that an enhanced pseudoscalar form factor, still consistent with measurements of the muon capture rate on ^{12}C, can double these estimates. The measured ratio of the exclusive to inclusive cross section is 11 ± 5 %; this is within expectation of the 5% ratio predicted in Refs. [2,4,8].

VII. CONCLUSION

An experiment has been performed to study the low-energy ν_μ-^{12}C interaction just above the muon threshold energy where nuclear effects dominate. A small sample of the events, with an observed ^{12}N decay, has been identified. Of the various theoretical predictions for the inclusive cross section with which the results have been compared, the FGM, modified to account for the final-state Coulomb interaction, is perhaps in best agreement. However, the measured outgoing muon kinetic-energy spectrum differs significantly from the FGM description. In addition, the measured cross section for the exclusive reaction ^{12}C$(\nu_\mu,\mu^-)^{12}$N(g.s.) is considerably higher than the calculations.

ACKNOWLEDGMENTS

This work was supported by the U.S. Department of Energy. We wish to thank the LAMPF and P-Division management at Los Alamos, L. Rosen, J. Browne, G. Stephenson, and F. Morse, for their support throughout the installation and operation of this experiment. We are grateful to T. W. Donnelly and J. S. O'Connell for pointing out to us the importance of the Coulomb correction in the FGM calculation, and to T. J. Haines for useful discussions. We want to acknowledge the help of A. Finch, D. Oakley, M. Baker, H. Concannon, and D. Anderson. One of us (G.J.V.) acknowledges support received from the University of California.

[1] J. D. Walecka, in *Muon Physics,* edited by V. W. Hughes and C. S. Wu (Academic, New York, 1975), Vol. II; in *Intersections Between Particle and Nuclear Physics,* Proceedings of the Conference, Steamboat Springs, CO, 1984, edited by R. E. Mischke, AIP Conf. Proc. No. 123 (AIP, New York, 1984).

[2] T. W. Donnelly, Proceedings of the Los Alamos Neutrino Workshop, Los Alamos National Laboratory Report No. LA-9358-C, 1981 (unpublished).

[3] R. Smith and E. Moniz, Nucl. Phys. **B43**, 605 (1972); J. S. O'Connell, in Ref. [2]; see also the Appendix in Ref. [5].

[4] H. Überall, B. A. Lamers, J. B. Langworthy, and F. J. Kelly, Phys. Rev. C **6**, 1911 (1972).

[5] T. Gaisser and J. S. O'Connell, Phys. Rev. D **34**, 822 (1986).

[6] B. Cortex *et al.*, in *Proceedings of the 1981 Orbis Scientiae, Gauge Theories, Massive Neutrinos, and Proton Decay,* edited by A. Perlmutter (Plenum, New York, 1981).

[7] C. Kim and S. L. Mintz, Phys. Rev. C **31**, 274 (1985). In this paper, the authors present a number of different cross-section estimates using different kinematic assumptions. For comparison, we have used their largest estimate.

[8] J. S. O'Connell, T. W. Donnelly, and J. D. Walecka, Phys. Rev. C **6**, 719 (1972): Updated values of some of the calculations can be found in Ref. [2].

[9] S. L. Mintz, Phys. Rev. C **25**, 1671 (1982).

[10] W.-Y. P. Hwang and H. Primakoff, Phys. Rev. C **16**, 397 (1977); W.-Y. P. Hwang, *ibid.* **20**, 805 (1979).

[11] We had expected more beam than was delivered to us, but poor running conditions and interference with the commissioning of the Proton Storage Ring reduced our beam allotment.

[12] W. Bauke, D. A. Clark, and P. B. Trujillo, Proc. Soc. Photo-Opt. Instrum. Eng. **483**, 131 (1984).

[13] T. Dombeck, A. Finch, and D. L. Grisham, Nucl. Instrum. Methods A **272**, 650 (1988).

[14] T. Kozlowski, J. F. Amann, G. T. Anderson, R. A. Floyd, J. F. Harrison, and M. A. Oothoudt, IEEE Trans. Nucl. Sci. **NS-30**, 3998 (1983).

[15] See, e.g., the review article "Energetic Muons" by M. G. Thompson, in *Cosmic Rays at Ground Level,* edited by A. W. Wolfendale (Institute of Physics, London, 1973).

[16] T. Suzuki, D. F. Measday, and J. P. Roalsvig, Phys. Rev. C **35**, 2212 (1987).

[17] T. Dombeck, Los Alamos National Laboratory No. LA-UR-1589, 1982 (unpublished); "A Proposal to the U.S. Department of Energy for a National Facility to Provide a High Intensity Neutrino Source," Los Alamos National Laboratory report, 1982 (unpublished).

[18] R. L. Burman, M. E. Potter, and E. S. Smith, Nucl. Instrum. Methods A **291**, 621 (1990).

[19] D. D. Koetke, Valparaiso University Report No. VU-PHY8901, 1989 (unpublished).

[20] D. R. F. Cochran, P. N. Dean, P. A. M. Gramm, E. A. Knapp, E. R. Martin, D. E. Nagle, R. B. Perkins, W. J. Shlaer, H. A. Thiessen, and E. D. Theriot, Phys. Rev. D **6**, 3085 (1972); J. F. Crawford *et al.*, Phys. Rev. C **22**, 1184 (1980); P. Denes, B. D. Dieterle, D. M. Wolfe, T. Bowles, T. Dombeck, J. E. Simmons, T. S. Bhatia, G. Glass, and W. G. Tippens, *ibid.* **27**, 1339 (1983).

[21] A. Wriekat, G. S. Adams, M. Bleszynski, S. M. Haji-Saeid, G. Igo, J. B. McClelland, G. Pauletta, C. A. Whitten, M. Gazzaly, and N. Tanaka, Phys. Lett. **97B**, 33 (1980); A. V. Dobrovolsky *et al.*, Nucl. Phys. **B214**, 1 (1983); H. B. Willard, B. D. Anderson, H. W. Baer, R. J. Barrett, P. R. Bevington, A. N. Anderson H. Willmes, and N. Jarmie, Phys. Rev. C **14**, 1545 (1976); G. S. Blanpied *et al.*, *ibid.* **18**, 1436 (1978); W. Schimmerling, T. J. Devlin, W. W. Johnson, K. G. Vosburgh, and R. E. Mischke, *ibid.* **7**, 248 (1973). The cross sections for protons on oxygen were scaled from those on carbon as $A^{2/3}$.

[22] W. R. Nelson, H. Hirayama, and D. W. O. Rogers, SLAC Report No. 265, 1985 (unpublished).

[23] J. Kang, Ph.D. thesis, University of New Mexico, 1987.

[24] E. J. Moniz, I. Sick, R. R. Whitney, J. R. Ficenec, R. D. Kephart, and W. P. Trower, Phys. Rev. Lett. **26**, 445 (1971).

[25] C. Tzara, Nucl. Phys. **B18**, 246 (1970).

[26] G. Epstein, M. Singham, and F. Tabakin, Phys. Rev. C **17**, 702 (1978).

[27] The observation of a muon energy spectrum softer than expected might provide an explanation for the anomalous ν_μ/ν_e ratio seen in atmospheric neutrino measurements. See K. S. Hirata *et al.*, Phys. Lett. B **205**, 416 (1988); K. S. Hirata *et al.*, *ibid.* **280**, 146 (1992); T. J. Haines *et al.*, Phys. Rev. Lett. **57**, 1986 (1986); D. Casper *et al.*, *ibid.* **66**, 2561 (1991); R. Becker-Szendy *et al.*, Phys. Rev. D **46**, 3720 (1992).

[28] S. L. Mintz and M. Pourkaviani, Phys. Rev. C **40**, 2458 (1989).

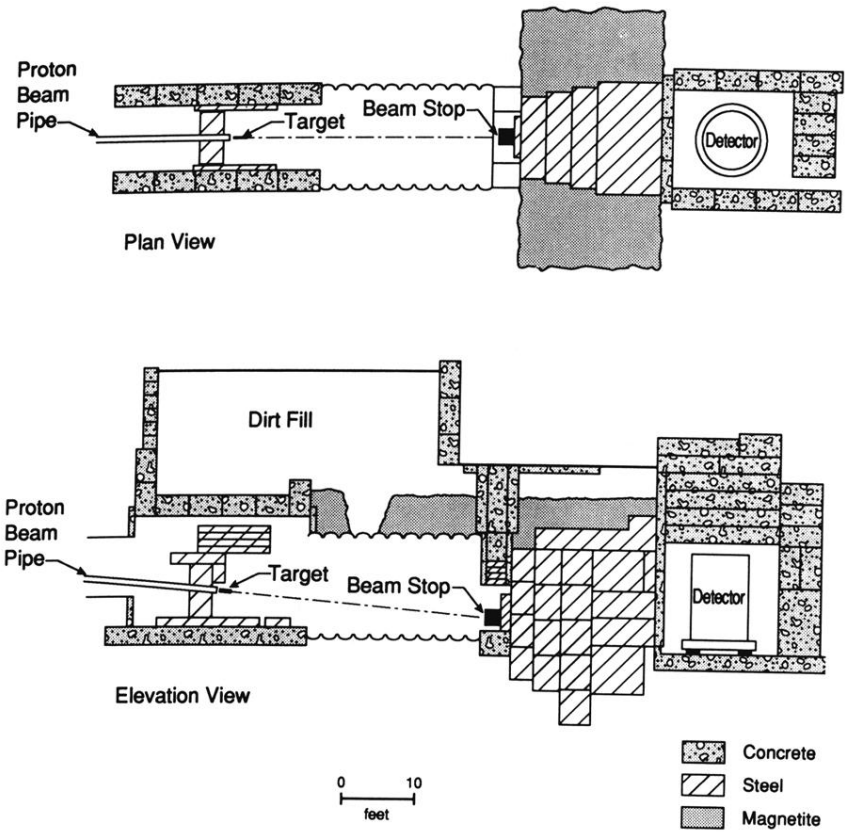

FIG. 1. The experimental setup is shown. Pions originating in the target decayed along the 12-m decay channel producing muon neutrinos. These struck the 5-ton scintillator detector which was set in a concrete bunker behind an 8-m-thick iron and magnetite shield.

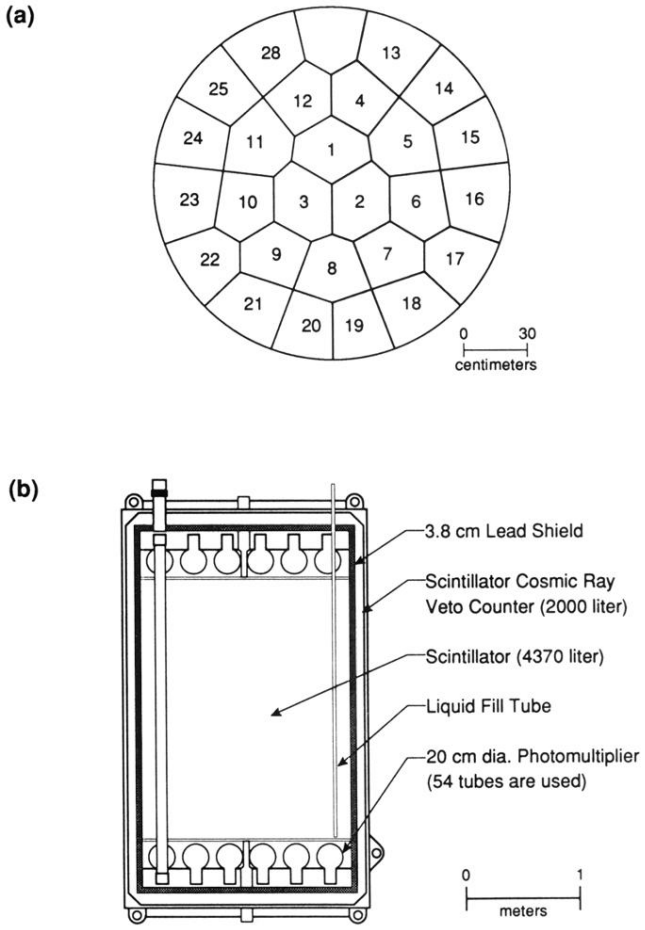

FIG. 2. (a) Neutrino detector top view indicating the 26 individual vertical modules. (b) Neutrino detector side view including the two active, liquid scintillator veto shields.

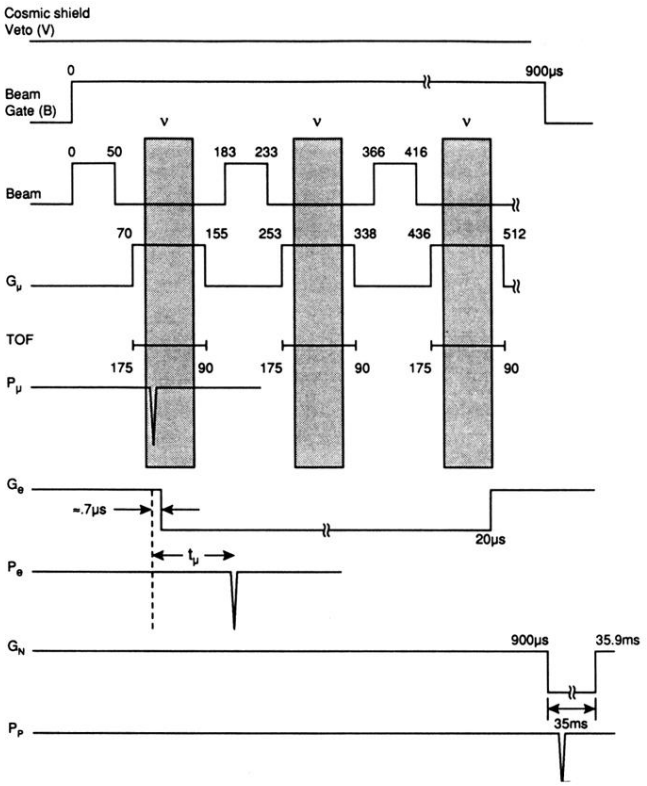

FIG. 4. Neutrino event gate sequence is shown. Note the breaks in the time axis and the changes in the time units.